OVERAGING, DEFORMATION AND RUPTURE MICROMECHANISMS OF ALLOY 718

IN RELATION TO NOTCH CREEP RUPTURE STRENGTH

R. Molins, E. Andrieu and A. Pineau
Centre des Matériaux, Ecole des Mines
B.P.87, 91003 EVRY Cédex (FRANCE)
URA CNRS N°860

Abstract

Long term (≃ 5000 hrs) creep tests were carried out on smooth and notched specimens of Alloy 718 at 650°C to investigate the effect of stress triaxiality and long exposures on notch rupture strength. In both notched specimens geometries which were tested, a notch strengthening effect is observed. A breaking point on the creep rupture curves is shown to coincide with the appearance of intergranular fracture at low applied stresses, especially in the notched specimens. The creep resistance is also shown to decrease at low applied stresses, when the times to failure are longer than approximately 2000 hours. The acceleration in the creep strain rate, which is associated with a decrease in the Norton law exponent, is related to the stability of the γ" phase which transforms to δ and to an increase in γ" particle size with time. A number of TEM observations suggest the existence of a stress-assisted coarsening effect. Other forms of intergranular microstructural modifications, including the precipitation of δ phase, Laves phases and Cr rich particles contribute also to the softening of the material and to the embrittlement of grain boundaries. Practical implications for extrapolating the creep resistance curves from short-term tests are briefly discussed.

Introduction

Alloy 718 is a material largely used in the fabrication of disks for gas turbines. These disks can experience exposures in operation of up to 40,000 hours at elevated temperatures (≃ 650°C). Rather surprisingly, except for few studies (see eg. [1]) very little has been published about the effects of long time stresses and temperatures on microstructural stability of Alloy 718.

In the specification of the creep strength of this material only short-term tests are currently performed on conventional smooth tensile specimens with therefore, a low stress triaxiality, which is not representative of the situation encountered in service, for instance along the firtree blade attachments of a disk . However, there also exist other specification tests carried out on creep notch specimens but these tests are only technical. In other materials, especially in steels, it has been shown that, in the

Superalloys 718, 625 and Various Derivatives
Edited by Edward A. Loria
The Minerals, Metals & Materials Society, 1991

presence of a notch which induces an increase in stress triaxiality ratio, it is possible to promote intergranular fracture (see eg.[2,3], for 316 stainless steel). The main objective of the present study was therefore to contribute to the knowledge of the behavior of this material when it is submitted to long exposure times in the presence of a notch and to compare the creep life of smooth bars and notched specimens. In the present study the results of creep tests which lasted up to about 10,000 hours are given. Such long exposures can induce microstructural modifications which were examined by Transmission Electron Microscopy (TEM). A better understanding of the aging behavior of γ' and γ'' strengthening precipitates and that of other phases formed under stress would also be important to predict the useful life of the components.

Material and experimental procedures

The chemical composition of the material is given in Table 1. This heat of Alloy 718,which was thoroughly investigated in the authors laboratory [4,5], was received as a wrought bar of 90 mm diameter. It was given a conventional heat-treatment : solution treated at 955°C for 60 min, then air-cooled + 720°C for 8 hours + Air cooled at 50°C/h down to 620°C + 620°C for 8 hours. This resulted in a grain size of about 30 µm with particles of the stable phase δ (Ni_3Nb) precipitated along the grain boundaries, as shown in Fig.1. The tensile properties measured at 20°C and 650°C are reported in Table 2.

Table 1 - Chemical composition (wt %).

C	Cr	Mo	Ti	Al	Nb+Ta	Fe	Si	Co	Mn	P	S	B
0.035	18.25	3.06	1.02	0.54	5.27	19.00	0.09	0.25	0.13	0.009	0.0015	0.006

Table 2 - Tensile properties.

Temperature (°C)	Yield Strength (MPa)	Tensile Strength (MPa)	Elongation A,(%)
20	1193	1377	20.3
650	964	1103	17.2

Creep tests were carried out at 650°C under an air environment using both Hydro-pneumatic and dead loadcreep frames. As a general rule radiation furnaces were used to heat the specimens which are shown in Fig.2. These specimens were cut along the longitudinal axis of the bar. A longitudinal or a diametral extensometer was used to measure the creep strain of the smooth bars or the notched specimens, respectively. In the latter case, the mean strain across the notch throat was defined as :

$$\bar{\epsilon} = 2 \text{ Log } (\Phi_o/\Phi) \qquad (1)$$

where Φ_o and Φ are the initial and the actual diameter of the minimum section, respectively.

Fig.2 shows that two notch geometries were selected with a notch of either 5 mm (FLE5 specimens) or 1 mm (FLE1 specimens). These geometries which lead

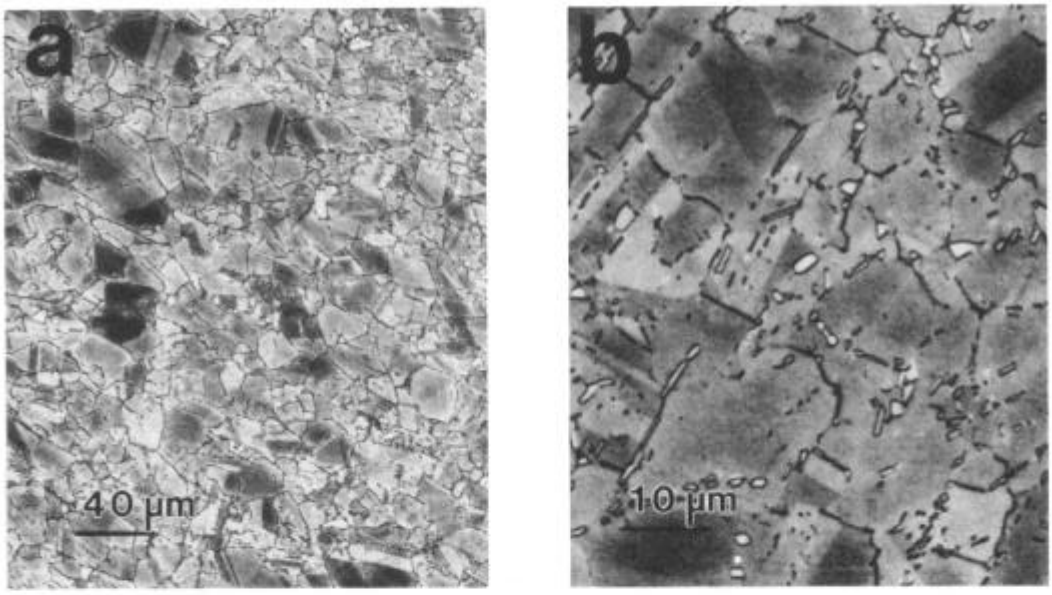

Figure 1 - a) General view of Alloy 718.b) Ni $_3$Nb particles precipitated along the grain boundaries.

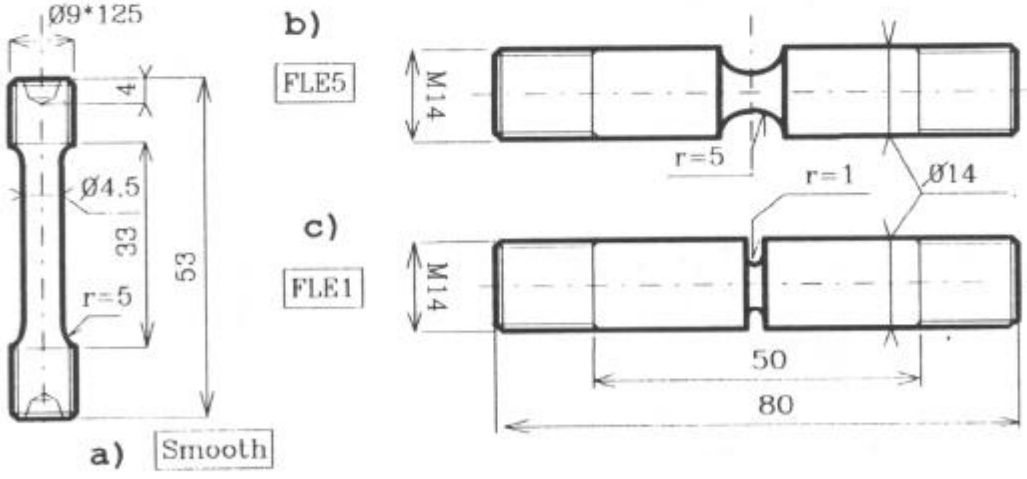

Figure 2 - Specimen geometries. a) smooth specimen; b) FLE1 specimen; c) FLE5 specimen.

to a stress concentration factor of $\simeq$ 1.30 (FLE5) and of $\simeq$ 3 (FLE1) were chosen because they have been largely investigated in the authors laboratory [2,3].

Scanning Electron Microscopy (SEM) and TEM were used to examine the fracture surfaces and the microstructure, respectively. Thin foils for TEM were prepared either from longitudinal or from transverse cuts in the smooth creep specimens. A special technique was also developed to prepare thin foils very close to the fracture surface in the minimum section of both types of notched specimens.

Results and Discussion

Mechanical tests

In Table 3, we have reported the results of creep tests performed on smooth and notched specimens. In this table, the nominal stress, σ_{nom} is defined as the applied load, P, divided by the initial section (minimum section for the notched geometries) of the specimens, t_R is the time to rupture, Σ is the reduction of area at failure, while $\bar{\epsilon}_F$ is the mean strain at rupture defined by Eq. (1).

Table 3 - Creep tests on smooth and notched specimens.

	σ_{nom} (MPa)	t_R (hours)	Σ (%)	$\bar{\epsilon}_F$ (%)
	750	39.5	54	77.6
S	700	97.5	59.9	91.4
M	650	198.2	64.2	102.7
O	600	645.5	62.6	98.3
O	575	718.6	65.5	106.9
T	530	1961.3	63.9	101.9
H	500	4158	70.2	121.1
	480	4348	69	117.1
	450	5429	74.5	136.6
	400	$\simeq$10.000	ND	ND

ND : Not Determined

		σ_{nom} (MPa)	t_R (hours)	Σ (%)	$\bar{\epsilon}_F$ (%)
		850	133	40.2	51.5
N		850	183	ND	ND
O		850	230	38.92	49.3
T	F	800	340	37.74	47.4
C	L	760	510	34.5	42.3
H	E	720	1240	34.68	42.6
E	5	650	1716	32.96	40
D		630	1954.8	35.98	44.6
		600	2717	36.87	46

	σ_{nom} (MPa)	t_R (hours)	Σ (%)	$\bar{\epsilon}_F$ (%)
	1100	226	24.04	27.5
F	998	738	20.78	23.30
L	930	1090	21.49	24.2
E	900	1890	22.19	25.1
1	850	1571	21.72	24.5
	800	2136	22.12	25

The variations of the time to rupture, t_R with the applied stress, σ_{nom} are shown in Fig.3 for the three geometries investigated. A notch strengthening effect is observed. This effect is equal to approximately 1.30 for the FLE5 specimens and to about 1.65 for the FLE1 geometry. A breaking point is also observed on the three σ_{nom}-t_R curves which gives rise to a steeper slope at large times to failure. It is worth noting that this change occurs at shorter times for the notched specimens compared to the smooth bars. In the latter case this change in slope takes place for $t_R \gtrsim 5000$ hours for an applied stress lower than about 500 MPa while it occurs in the FLE1 specimens for $t_R \gtrsim 800$ hours. The results reported in Table 3 indicate that the creep ductility of the notched specimens is much smaller than the creep rupture strain measured on smooth specimens. It is also observed that, for a given specimen geometry, the creep ductility is almost independent of the time to failure.

The variations of the minimum creep strain rate, $\dot{\epsilon}$ with the applied stress, measured on smooth specimens, are reported in Table 4 and shown in Fig.4 where a change in slope is also observed to take place for an applied stress between 500 and 600 MPa. If the creep strain rate, $\dot{\epsilon}$ is written as a Norton law, that is :

$$\dot{\epsilon} = k \sigma^n \qquad (2)$$

it is found that n = 13.6 for large applied stresses (> 600 MPa), which is a usual value for Alloy 718 determined in specification tests. On the other hand, at low applied stresses (σ < 500 MPa), the n exponent is much lower, on the order of 5.9 for 400 MPa $\leqslant \sigma <$ 500 MPa. It is clear that tests performed at still lower stresses might lead to smaller values of the n exponent. It is also worth noting that an extrapolation of the creep law determined at large applied stresses (n = 13.6) would lead to a significant underestimate of the creep strain rate, by an order of magnitude for $\sigma \simeq$ 400 MPa.

Table 4 - Minimum creep strain rate on smooth specimens as a function of applied stress.

σ_{nom} (MPa)	750	700	650	600	575	500	480	450	400
$\dot{\epsilon}$ (hr^{-1})	2.56 x 10^{-4}	7.10 x 10^{-5}	3.21 x 10^{-5}	1.32 x 10^{-5}	6.51 x 10^{-6}	1.80 x 10^{-6}	1.60 x 10^{-6}	1.10 x 10^{-6}	7.50 x 10^{-7}

This progressive variation of the creep resistance is also observed on a Monkman-Grant diagram. Two main regimes can be defined, as shown in Fig.5, where a simple relationship between the minimum creep strain rate, $\dot{\epsilon}$ and the time to rupture, t_R is written as :

$$\underset{(h^{-1})}{\dot{\epsilon}^{\alpha}} \cdot \underset{(h)}{t_R} = C_m \qquad (3)$$

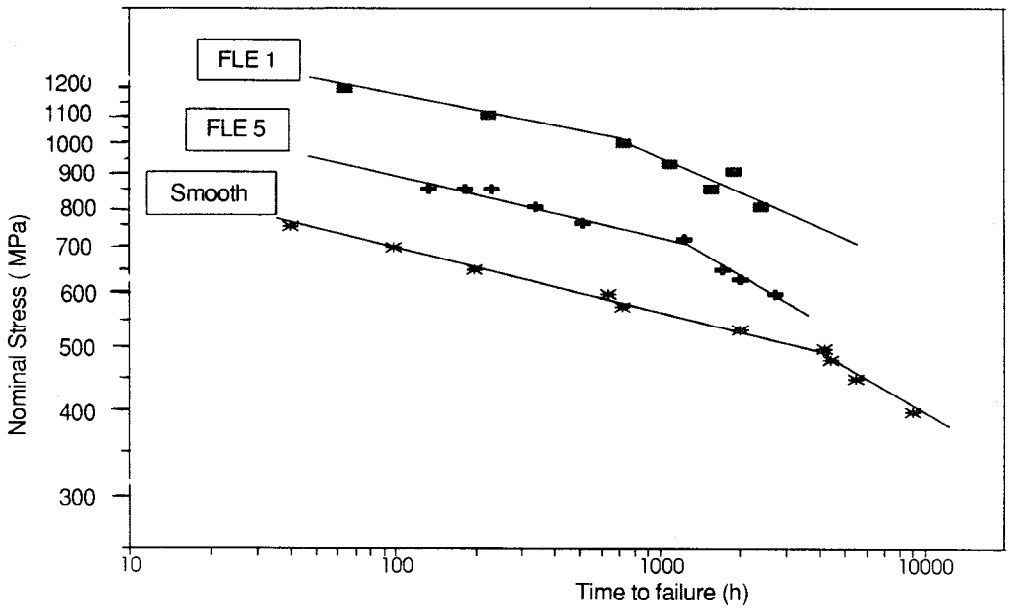

Figure 3 - Variation of the applied stress σ_{nom} with the time to rupture t_R for the three specimen geometries. Effect of a notch strengthening.

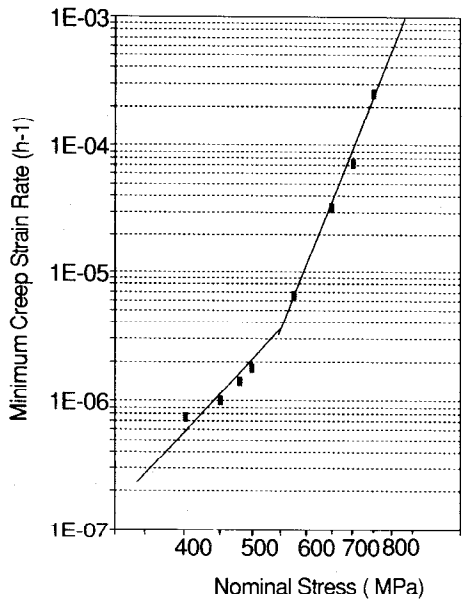

Figure 4 - Variation of the minimum creep strain rate with the applied stress for smooth specimens.

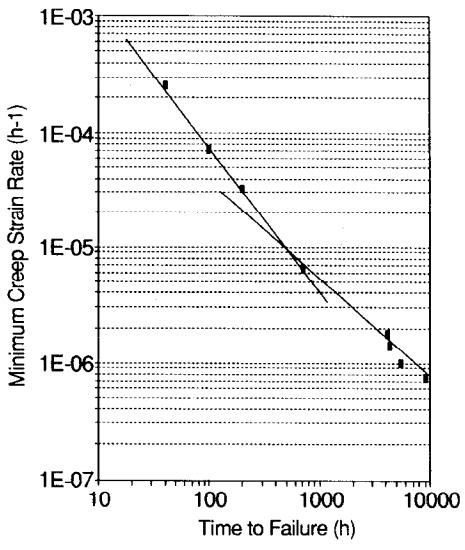

Figure 5 - Variation of the minimum creep strain rate with the time to rupture for smooth specimens.

At large applied stresses, ie for $t_R < 1000$ hours, it is found that $\alpha = 0.70$ and $C_m = 4.710^{-2}$, while at lower stresses, ie for $t_R > 1000$ hours, $\alpha = 1.21$ and $C_m = 4.310^{-4}$. The creep damage tolerance factor defined by :

$$\lambda = \epsilon_R / \dot{\epsilon}\ t_R \qquad (4)$$

is large and shows no significant change over the stress range investigated. The value of the Monkman Grant index, defined by the product $\dot{\epsilon}\ t_R \simeq 5.10^{-3}$ is lower than the value of the ratio $1/n = 7.510^{-2}$. This suggests that, under uniaxial tensile deformation, tertiary damage is essentially due to uniform straining and the progressive formation of a diffuse neck [6]. This conclusion applies essentially to short-term creep tests ($t_R \lesssim 5000$ hours), that is for the majority of the experiments which were performed on smooth specimens.

Hardness measurements made on specimens taken from the heads of creep specimens showed no significant change. The Vickers hardness, measured under an applied load of 200 N, remained constant ($\simeq$420) even for exposure times longer than 5000 hours. Similar measurements carried out on the gage length of creep specimens showed an influence of the applied stress and therefore of the test time. It was observed that, for the same creep strain, the hardness of the specimens which were submitted to a low applied stress was smaller than that of the specimens tested at larger stresses. For example, for a creep strain of 20%, the hardness of a specimen tested at $\sigma = 650$ MPa ($t_R \simeq 200$ hours) was about 510 HV, while the hardness of a specimen submitted to an applied stress of 450 MPa ($t_R \simeq 5500$ hours) was only 485 HV. This strongly suggests that microstructural modifications are taking place within the material after long time exposures under an applied stress.

Fractography and fracture modes

SEM observations showed that the fracture surfaces of smooth specimens, even those which were tested at the longest times to rupture, were covered by transgranular ductile dimples, as shown in Fig.6. Most of these dimples observed in the center of this cup-and-cone fracture were initiated from carbides, as suggested by the observation of longitudinal sections prepared close to the fracture surface (Fig.6b). Thus in the smooth specimens, at least for $t_R \lesssim 5000$ hours , no evidence of intergranular fracture could be shown.

The situation was completely different in the notched specimens, as illustrated in Fig.7 where longitudinal sections of FLE5 type specimens are shown. It is observed that, at large applied stress, the failure mode remains essentially ductile and transgranular, as in smooth specimens. Transgranular cavities are initiated from carbides. On the other hand at lower applied stress, beyond the breaking point on the σ_{nom}-t_R curve the failure mode is partly intergranular, as shown in Fig.7b where a number of cavities initiated from grain boundary facets can be observed. In FLE5 and FLE1 specimens the stress triaxiality measured by the ratio between the mean stress, σ_m and the equivalent Von-Mises stress is about 0.60 and 1, respectively, compared to 1/3 in the smooth bars. These observations show therefore that an increase in stress triaxialityratio tends to promote intergranular damage, which might be, at least partly, responsible for the change in the slope of the σ_{nom}-t_R curves. It should also be noted that fracture took place at the center of the specimens, which means that there is no environmental effect in the results of these tests.

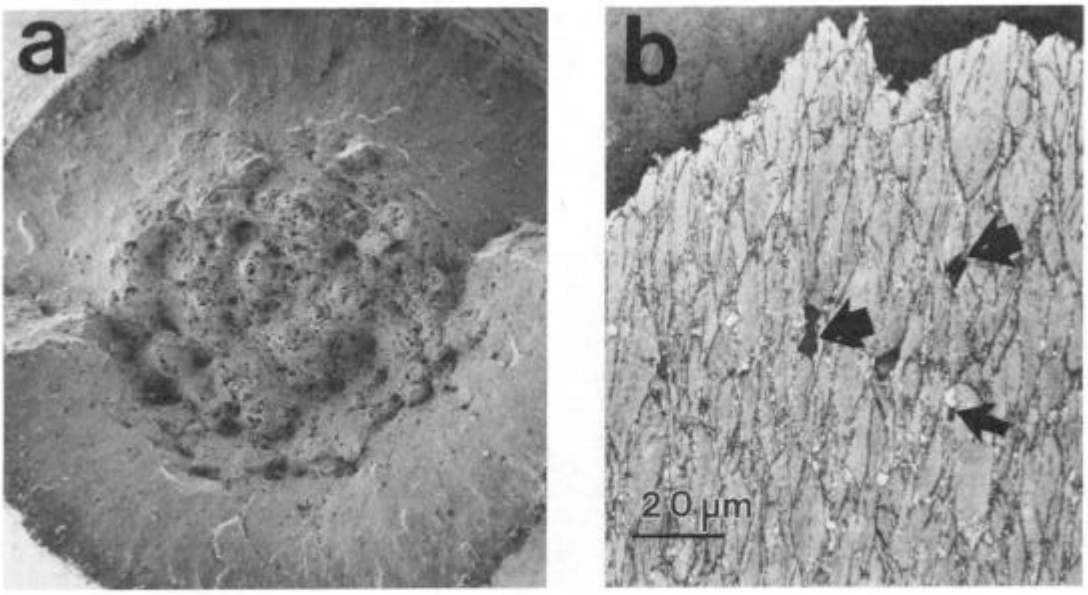

Figure 6 - a) SEM observation of a smooth specimen surface fracture. σ_{nom} = 450 MPa - t_R = 5429 hrs; b) longitudinal section. The arrows indicate the position of cavities initiated from carbides.

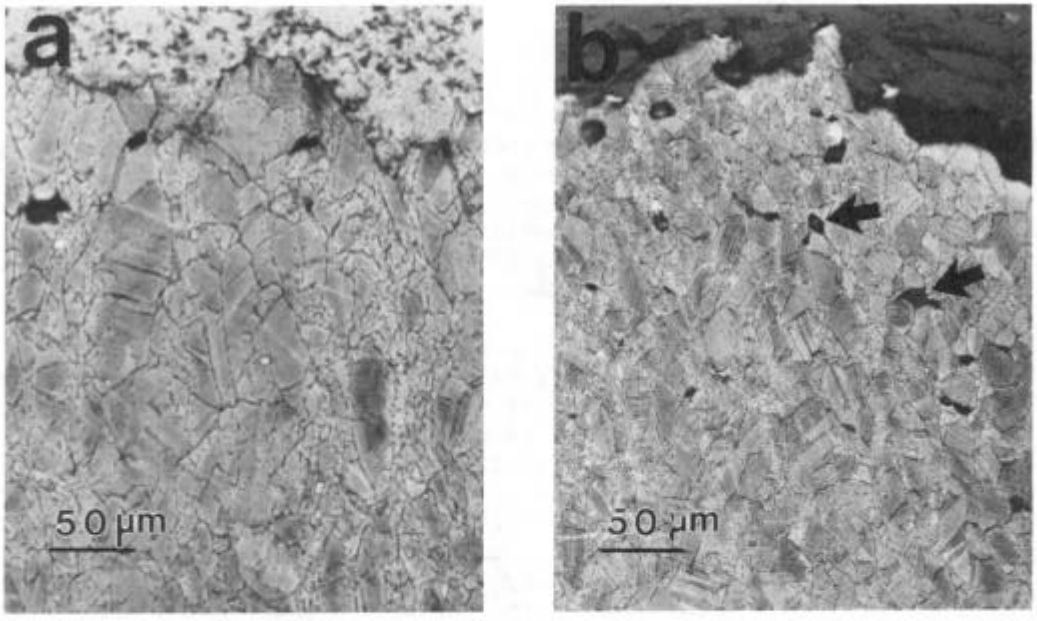

Figure 7 - SEM observation of a notched specimen (FLE5) longitudinal section for two applied stresses. a) σ = 800 MPa; t_R = 340 hrs; b) σ = 600 MPa; t_R = 2717 hrs. The arrows indicate the position of cracked grain boundaries.

TEM observations

In Alloy 718 the dislocation substructures are difficult to observe because of the pronounced contrasts associated with coherency strains between the γ' and γ'' particles and the matrix. In many circumstances planar defects similar to those shown in Fig.8 could be identified. These defects are formed by mechanical microtwins and planar defects in the γ'' precipitates which are initiation sites for the formation of the stable δ orthorhombic phase, as shown earlier [7-9]. It is thus confirmed that, in this material, low strain rates tend to promote planar slip which, in turn, might be partly responsible for slip-induced intergranular fracture [10].

In the present study the emphasis was laid on the effects of applied stress and long time exposures on microstructural modifications. The results related to both transgranular and intergranular overaging are successively presented.

Transgranular overaging

Two main overaging phenomena were observed :(i) the formation of transgranular δ phase, as shown in Fig.8 and 9, where denuded zones of γ'' precipitates are formed around relatively long δ platelets, and (ii) the increase in precipitate size (Fig.10). This figure shows the variations of the mean value of the length, L of isolated γ'' precipitates measured in a <100> direction. These measurements were made on thin foils cut in the head of the specimens (stress free condition). However, one result obtained on a thin foil taken in the center of a FLE5 specimen is also reported. In this figure we have also included one result derived from the observation of the pictures published by Radavich [1] who examined also the effect of long time stresses on microstructural stability of Alloy 718. Fig.10 shows that, in the absence of any applied stress, the γ'' size, $\bar{L}$ increases with time, approximatively as $t^{1/2}$. This result applies essentially to isolated γ'' precipitates since it was observed that, when the γ' and γ'' particles were associated, the coarsening rate of the precipitates was reduced, as expected from the earlier work carried out in our laboratory on the γ'-γ'' compact morphology [10,11] and from more recent studies on modified compositions of Alloy 718 [12,13].

Very little is known about the coarsening behavior of γ'' precipitates. One should be tempted to think that the usual coarsening law derived by Lifshitz, Slyozov [14] and Wagner [15] (LSW), which states that the mean volume of the particles is proportional to time, should also be obeyed, that is, within a first approximation, the product L^2e, where e is the thickness of the disk-shaped precipitates, should be proportional to time. In the present study the variation of the thickness, e with L was not determined. However in a previous study dealing with γ'' precipitates in a Fe-Ni-Ta alloy, it was shown that the aspect ratio of the particles, e/L was a decreasing function of L [16]. The observed coarsening rate suggests that e/L should be roughly inversely proportional to L, which is a variation slightly larger than that observed previously in the Fe-Ni-Ta alloy. This difference might be related to the difference in coherency strains and interfacial energy between the matrix and the precipitates.

Fig.10 shows another interesting result which is a stress-enhanced coarsening rate effect. Very little is also known about this effect. One possible explanation for this phenomenon could rely on a stress-assisted dissolution of one of two variants of the γ'' precipitates, as observed by Oblak, et al [17] on single crystals of Alloy 718. These authors showed that a tensile stress applied along the [001] direction leads to the

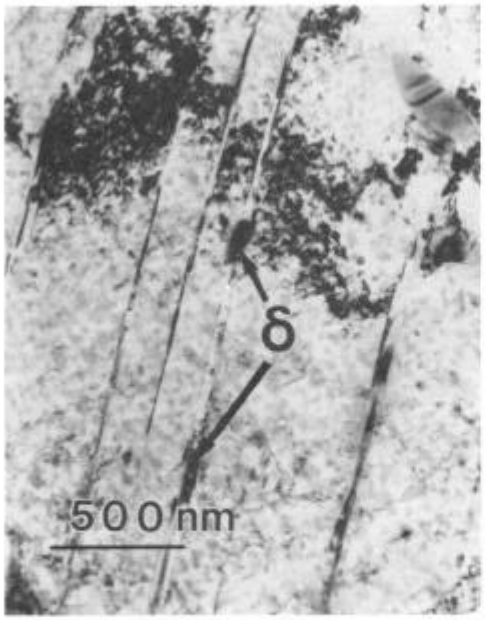

Figure 8 - TEM observation of planar defects in the matrix. FLE5; σ_{nom} = 600 MPa; t_R = 2717 hrs.

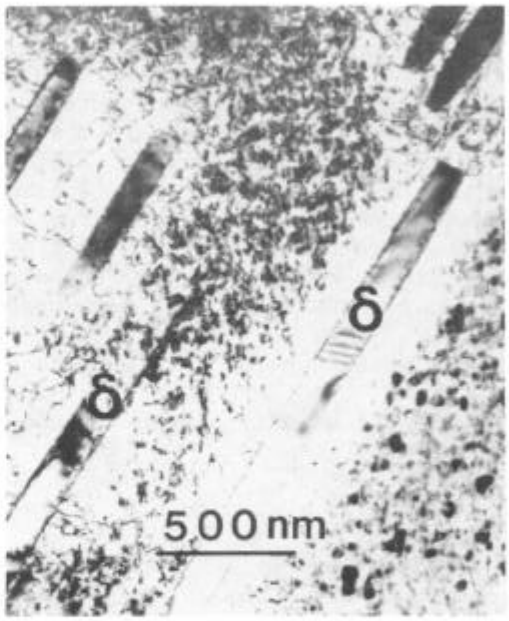

Figure 9 - TEM observation of transgranular δ phases surrounded by γ" precipitate denuded zones.

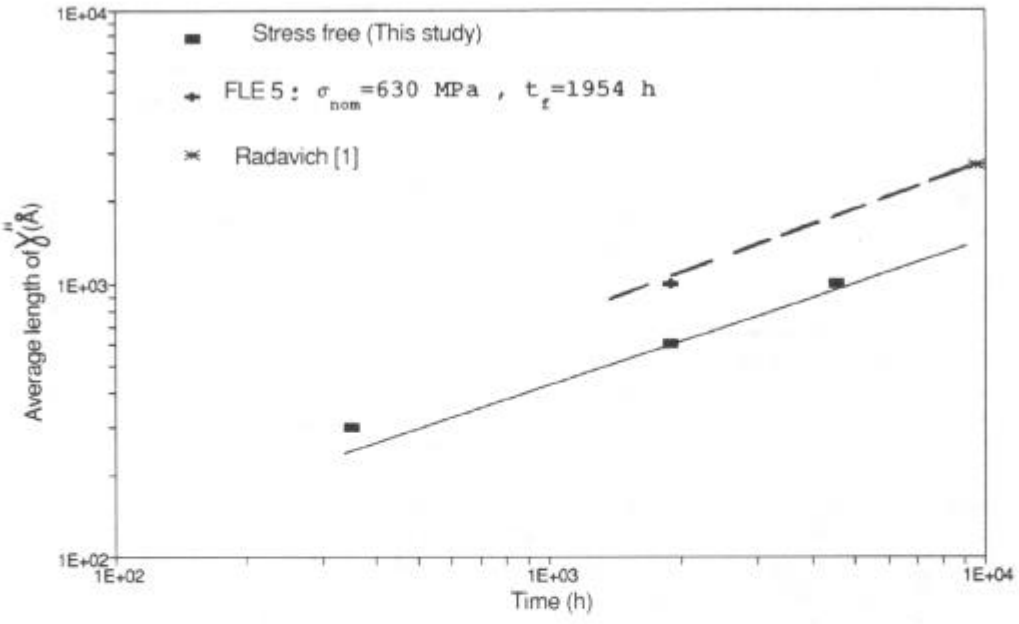

Figure 10 - Variation of the length of isolated γ" precipitates during overaging.

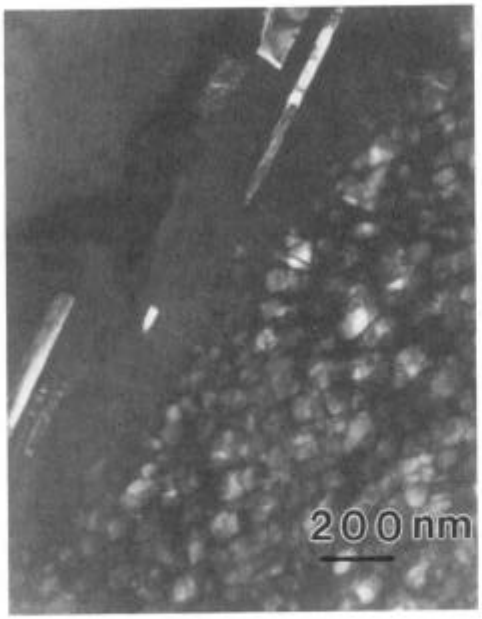

Figure 11 - TEM observation of γ'' depletion along a δ phase decorated grain boundary. FLE5; σ_{nom} = 600 MPa; t_R = 2717 hrs.

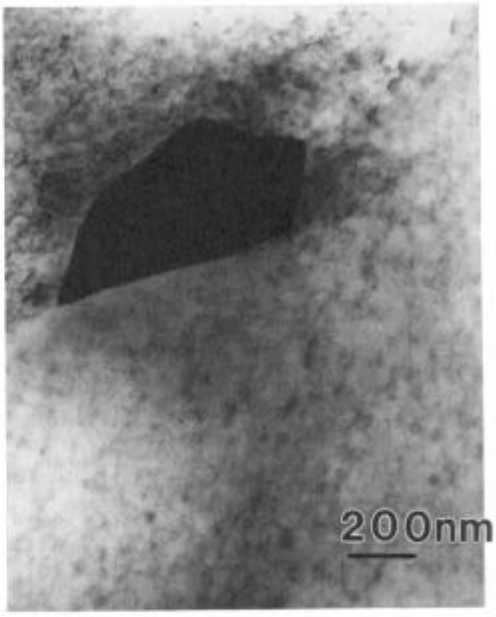

Figure 12 - TEM observation of a Laves phase precipitated along a grain boundary.

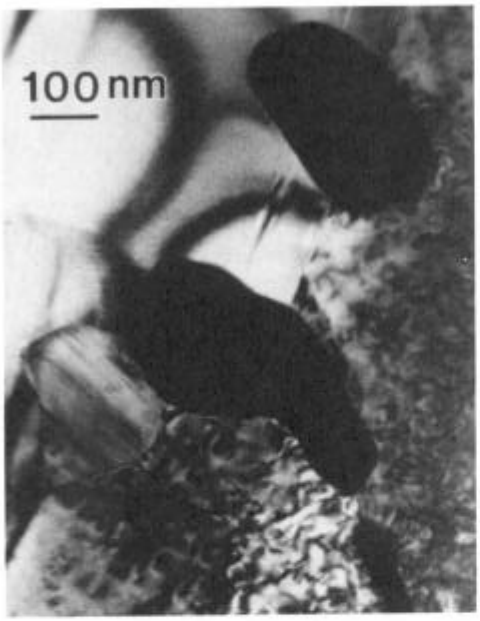

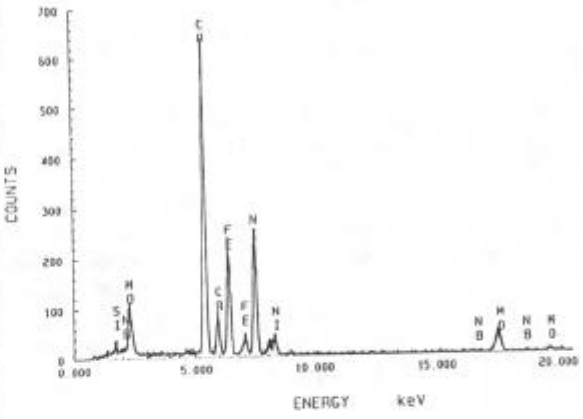

Figure 13 - Analytical TEM characterization of an intergranular chromium rich phase.

dissolution of the two variants for γ'' precipitates with their $\vec{c}$ axis aligned along the [100] and [010] directions. A close examination to a number of TEM pictures taken on specimens which were submitted of an applied stress or to Fig.3 published by Radavich [1] suggests that the three variants of γ'' precipitates are not evenly developed. Further work is needed to conclude more quantitatively on the stress-assisted coarsening behavior of Alloy 718.

Both forms of transgranular overaging effect are likely to be responsible for the increase in creep strain rate observed at low applied stresses (Fig.4). Chaturvedi and Han [18] showed that in Alloy 718 the creep strain rate at 600°C is an increasing function of precipitate size when the particles are larger than 30 nm, which is the situation corresponding to our longtime test conditions (Fig.10). The fact that the value of the stress exponent in the creep rate equation (Eq.2) increases with applied stress might also be related to a change in the creep deformation mechanisms, from linear or diffusional creep to dislocation power law creep when the applied stress is increased. This latter explanation is all the more likely as grain boundary microstructural modifications are also taking place after long time exposures, as shown in the next section.

Intergranular overaging

It has already been shown that in Alloy 718 longtime stresses and temperatures produce a number of microstructural grain boundary modifications [1]. The first modification is the precipitation of δ phase along the grain boundaries with the formation of a denuded zone of γ'' precipitates (Fig.11). This picture shows that the grain boundaries can be "weakened" over a small distance of about 100 nm. This might induce ductile intergranular fracture because of the localization of the creep strain in the softened denuded zones. The second modification is the precipitation of other phases which are not present in the initial conditions. Two kinds of these new phases were identified : (i) the Laves phase, Fe_2 (Mo,Nb) shown in Fig.12, and (ii) the precipitation of blocky particles (Fig.13) which were identified as a phase rich in chromium (Fig.13b).

These intergranular precipitation reactions contribute to the weakening of the matrix because of the decrease in solute content, especially Mo and Cr, and thus to the increase in the creep strain rate observed at low applied stresses (Fig.4). They can also initiate the formation of creep cavities. The growth rate of these cavities is dependent on the maximum principal stress, σ_{zz}, when the growth mechanism is diffusion controlled. This might explain why the transition in the σ_{nom} - t_R curves, which is largely associated with the appearance of intergranular fracture, occurs at much shorter times on the notched geometries since, in these specimens, σ_{zz} is larger than in smooth bars.

Conclusions

1. In Alloy 718 longtime exposures at 650°C produce a number of microstructural modifications which strongly affect the creep resistance of this material. A number of intergranular precipitation reactions, including the formation of δ phase, Laves phase and a Cr rich phase contribute to the softening of the material. Transgranular overaging is associated with the precipitation of δ platelets along planar slip bands leading to the formation of denuded zones of strengthening γ'' precipitates. Measurements of particle size show that the coarsening rate of γ'' precipitates would be proportional to (time) $^{1/2}$ and, more importantly, would be enhanced by an applied stress.

2. These transgranular microstructural modifications lead to a decrease in the stress exponent of the creep Norton law and to an increase in the creep strain rate. A change in the creep deformation mechanisms, from dislocation power low creep to diffusionnal creep when the applied stress is decreased might also contribute to the change in the stress exponant of the Norton law.

3. The failure mode of smooth creep specimens is essentially transgranular, even for times to failure as long as 5000 hours. On the other hand, a transition in the failure mode, between transgranular at large applied stresses and predominantly intergranular at low applied stresses is observed on notched specimens. This transition time which is observed on the creep rupture curves is a decreasing function of the stress triaxiality ratio.

4. These results underline the difficulties associated with the extrapolation of accelerated creep tests carried out on smooth bars to predict the useful life of components.

Acknowledgments

The authors would like to acknowledge the Snecma Compagny who showed a constant interest in this study.

References

1. J.F. Radavich, "Long time stability of a wrought alloy 718 disk. Superalloy 718 - Metallurgy and Applications, Ed. by E.A. Loria, The Minerals, Metals and Materials Society, (1989), 257-268.

2. M. Yoshida, C. Levaillant, R. Piques and A. Pineau, "Quantitative study of intergranular damage in an austenitic stainless steel on smooth and notched bars. High Temperature Fracture. Mechanisms and Mechanics, Ed. by P. Bensussan and J.P. Mascarell, EGF Pub.6, MEP (1990), London, 3-21.

3. M. Yoshida, C. Levaillant and A. Pineau. "Metallographic measurement of creep intergranular damage and creep strain. Influence of stress state on critical damage at failure in an austenitic stainless steel". Int. Conf.on Creep, Tokyo, (1986), 327-332.

4. A. Diboine and A. Pineau, Fatigue and Fracture of Engineering, Materials and Structure, vol.10, (1987), 141-151.

5. A. Diboine, "Etude de la propagation des fissures en fatigue-fluage-oxydation à 650°C dans un superalliage base nickel : l'Inconel 718". Thesis Ecole des Mines, (1985).

6. P. Bensussan, "Approches mécaniques globale et locale de l'amorçage et de la propagation de fissures par fluage dans l'alliage léger Al-Cu 2219". Thesis, ORSAY (France), (1986).

7. D. Fournier and A. Pineau, "Low cycle fatigue behavior of Inconel 718 at 298 K and 823 K. Metall. Trans. vol.8A, (1977), 1095-1105.

8. M. Clavel, D. Fournier and A. Pineau, "Plastic zone sizes in fatigued specimens of Inco 718. Metall. Trans., vol.6A, (1975), 2305-2307.

9. M. Clavel and A. Pineau, Mat. Sci. and Eng., vol.55, (1982), 157-171 and 173-180.

10. E. Andrieu, R. Cozar and A. Pineau. "Effect of environment and microstructure on the high temperature behavior of ALloy 718". Superalloy 718 - Metallurgy and Applications, Ed. by E.A. Loria, The Minerals, Metals and Materials Society, (1989), 241-256.

11. R. Cozar and A. Pineau, "Morphology of γ' and γ'' precipitates and thermal stability of Inconel 718 Type alloys", Metall. Trans., vol.4A, (1973), 47-59.

12. E. Guo, F. Xu and E.A. Loria, "Improving thermal stability of alloy 718 via small modifications in composition". Superalloy 718 - Metallurgy and Applications, Ed. by E.A. Loria, The Minerals, Metals and MaterialsSociety, (1989), 567-576.

13. J.P. Collier, S.H. Wong, J.C. Phillips and J.K. Tien, "The effect of varying Al, Ti and Nb content on the phase stability of Inconel 718", Metall. Trans., vol.19A, (1988), 1657-1666.

14. I.M. Lifshitz and V.V. Slyozov, J. Phys. Chem. Solids, vol.19, (1961), 35.

15. C. Wagner, Z. Elektrochem., vol.65, (1961), 581.

16. R. Cozar and A. Pineau. "Influence of coherency strains on precipitate shape in a Fe-Ni-Ta alloy", Scripta Metall., vol.7, (1973), 851-854.

17. J.M. Oblak, D.F. Paulonis and D.S. Duvall, "Coherency strengthening in Ni base alloys hardened by $DO_{22}\gamma''$ precipitates". Metall. Trans., vol.5, (1974), 143-153.

18. M.C. Chaturvedi and Y. Han, "Creep deformation of Alloy 718". Superalloy 718 - Metallurgy and Applications", Ed. by E.A. Loria, The Minerals, Metals and Materials Society, (1989), 489-498.